

Characterization and Modeling of Spot-Weld Joints in Press Hardening Steels Associated with Softening in Heat Affected Zone

Hassan Ghassemi-Armaki¹, Qaiser Khan¹, Amandeep Singh Gill², Scott Zilincik²

¹ArcelorMittal Global R&D, East Chicago, IN, USA

²FCA Chrysler Technical Center, Auburn Hills, Michigan, USA

Next generation of advanced high strength steels (AHSS) are extensively considered for usage in Body-in-White (BIW) with lower thickness to reduce the vehicle weight and increase fuel efficiency. Resistance Spot Welding (RSW) continues to be a major joining process in BIW, with an average of 4500 spot-welds per vehicle. Spot-weld strength has direct correlation with the thicknesses, and yield strength of the joining sheets in the stackup configuration.

Characterization and FEA modeling of spot-welds for accurate failure prediction is of vital importance in vehicle crash safety simulations. This will also lead to an optimized weld layout, optimum weld pitch and cycle time and this has a direct impact on assembly plant layout/investment. Press Hardening Steels "PHS" (e.g. Usibor® 1500) show high strength after hot-stamping and are one of the major category of AHSS. These steels contain a fully martensitic microstructure, which show softening in Heat Affected Zone (HAZ) after spot-welding because of martensite tempering. Accurate prediction of load-displacement and failure load of the spot-weld depends on input data for softened HAZ and connection definition of two joining sheets.

In the present study, a modeling method for the spot-weld nugget and HAZ zone was developed and compared to test results. An eight, hexahedral element assembly is used to represent a spot-weld and an element ring of width, 0.35 times of the weld diameter is used to simulate softened HAZ. Since softening in the HAZ is not uniform and shows a gradient as a function of distance from spot-weld center, the HAZ material simulated using Gleeble for different locations was used to characterize and provide material input data for the HAZ shell element.

Spot-weld failure was characterized by testing the spot-weld in different loading modes, including, tension-shear, coach-peel, cross-tension and KSII configurations (30, 60 and 90 degrees). *MAT_100_DA in LS-DYNA (version 9.1) was used along *DEFINE_CONNECTION_PROPERTIES for defining material properties for the weld. Results show that the chosen stress-strain curve representative for HAZ shell elements extracted from Gleeble samples can predict the yielding of the load-displacement curve well. Additionally, *MAT_100_DA parameters depend on sheet metal thickness, and exponents for failure equation in this model can be lower than 1 and up to 4 as reported in literature.

1 Introduction

AHSS with strengths above 1000 MPa are of particular interest to the automotive market. They can be used to improve crash performance, while reducing gauge for weight reduction and consequently increasing fuel efficiency. Press-Hardening Steels (PHS) are one of the important AHSS grades that can be formed easily at high temperature and show high strength at room temperature. These materials are extensively used in BIW applications and are spot welded to similar or different high strength steels. Virtual prediction of welded structures for crashworthiness has attracted significant attention from investigators in both industry and academia. A weld must be able to sustain a load until it yields and then dissipate kinetic energy from impact in a controlled manner [1]. A precise predictive model provides cost and time savings in a vehicle development cycle by reducing the number of experiments [2].

The spot-weld material is simulated with an isotropic hardening plasticity model. Failure of spot-weld elements is based on a two dimensional (2D) or three dimensional (3D) failure surface, which is either force or stress based. In these models, a spot-weld element is deleted when force or stress goes beyond the failure surface. Force-based failure surface depend on nugget diameter, and individual material cards should be made and implemented for each identified stackup [1-4]. 2D failure surface models are mostly based on shear and axial forces which can be measured by KSII tests at

zero and 90 degrees respectively. Typical cross-tension and tension-shear tests described in all standard weld tests can also be used for predicting these forces. However, there is bending of the base material that occurs around the nugget during these tests, and consequently maximum loads extracted from these tests are not pure shear or axial. To overcome this, Lim et al, used a hybrid experiment and inverse FEA modeling to predict failure loads for different loading modes [4]. Equations 1 and 2 are two major failure models used in this category.

$$\left(\frac{f_n}{F_n}\right)^m + \left(\frac{f_s}{F_s}\right)^m = 1 \quad (1)$$

where F_n and F_s are axial force and shear force at failure in test; while f_n and f_s are axial and shear force experienced by the spot weld in FEA model [5].

$$f = \left(\frac{\sigma_N}{S_N(\dot{\epsilon}_{eff})}\right)^2 + \left(\frac{\tau}{S_S(\dot{\epsilon}_{eff})}\right)^2 \geq 1 \quad (2)$$

where σ_N and τ are weld axial and shear stresses; and $S_N(\dot{\epsilon}_{eff})$ and $S_S(\dot{\epsilon}_{eff})$ are strain rate dependent axial and shear stress limits. 3D failure surfaces include a moment (force-based) or bending stress (stress-based) component as well. The moment and bending stress are calculated by using a coach-peel test and inverse FEA modeling. Failure of spot-welds in AHSS is more sensitive to the moment, and it is important to capture the effect of moment in combination with the axial and shear loading components. Equations 3 and 4 are two major 3D failure models used in LS-DYNA [6].

$$f = \left(\frac{N_{rr}}{N_{rrF}}\right)^2 + \left(\frac{N_{rs}}{N_{rsF}}\right)^2 + \left(\frac{N_{rt}}{N_{rtF}}\right)^2 + \left(\frac{M_{rr}}{M_{rrF}}\right)^2 + \left(\frac{M_{ss}}{M_{ssF}}\right)^2 + \left(\frac{M_{tt}}{M_{ttF}}\right)^2 \geq 1 \quad (3)$$

where rr , rs , and rt represent axial, hoop, and radial directions respectively. N_{rr} , N_{rs} and N_{rt} are force resultants, while N_{rrF} , N_{rsF} and N_{rtF} are force resultants at failure specified by users; M_{rr} , M_{rs} and M_{rt} are moment resultants and M_{rrF} , M_{rsF} and M_{rtF} are moment resultants at failure specified by users. Equation 3 is force-based and referred to by the MAT_100 material card in LS-DYNA [4, 6].

$$f = \left(\frac{\sigma_N}{S_N(\dot{\epsilon}_{eff})}\right)^{n_N} + \left(\frac{\sigma_B}{S_B(\dot{\epsilon}_{eff})}\right)^{n_B} + \left(\frac{\tau}{S_S(\dot{\epsilon}_{eff})}\right)^{n_S} \geq 1 \quad (4)$$

Equation (4) is a stress-based failure model where σ_B is the bending stress and used in *MAT_100_DA material card. In a 3D force-based material model (Eq. 3), all forces in different loading modes that contribute to failure are inserted separately, while as in a 3D stress-based material model (Eq. 4), all forces are converted to three major stresses - shear stress, normal stress and bending stress. Torsion is included in the model as part of shear stress [4, 6]. Strain-based failure has been studied for joint failure and is more appropriate for ductile failure. In these models, a weld element is eliminated when effective plastic strain exceeds a certain critical strain. Bier et al used MAT_024 for failure of the hexahedral elements representative of rivet joints with a constrained contact (i.e. *CONSTRAINED_TIE_BREAK) in which a solid element fails based on a critical plastic strain [2].

In a full vehicle crash, spot-welds and HAZ are under complex stress/strain state. Simultaneous bending and stretching of a component in crash test results in strain localization in the softened HAZ, which causes a premature fracture initiation. Consequently, crack propagation into neighboring base material leads to loss of structural integrity [7]. Preliminary studies have used

vickers hardness across spot-weld specimens to generate plasticity data for HAZ by using a scale factor between the base material and HAZ hardness [8]. These methods may give a good prediction of ultimate tensile strength, but not in yielding onset, or strain hardening. With the scaling factor method, strain hardening doesn't change and the yield point decreases in a trend similar to the ultimate tensile strength. However, studies with specimens of HAZ simulated using Gleeble show that, in the HAZ, strain hardening decreases considerably with mild tempering, while the yield point increases with initial tempering and does not reduce compared to base material yield point [9].

Eller et al investigated the effect of softened HAZ on strain hardening and fracture strain [7]. For calibration of the strain hardening in the HAZ, they developed a specially designed asymmetric uni-axial tensile specimen, and used the measured force–displacement curves and the strain fields as input for an inverse FEM optimization. The algorithm identified the strain hardening model parameters by minimizing the differences between experimental and simulated results [7, 10]. They also calibrated a strain-based fracture model using a hybrid experimental/numerical approach. Strain hardening and fracture strains were assumed to be linearly related to the as-welded material hardness [7]. However, the identification of the parameters using inverse FEM optimization and calibration were done by using a very fine solid mesh of 0.1-0.5 mm element size. While the method is valuable for strain hardening parameters identification, shell elements of much bigger size are used in full vehicle CAE models and HAZ cannot be partitioned to such a small size. Hence, fracture strain should be averaged to capture failure and damage for the entire HAZ with one shell element. Sommer et al simulated HAZ microstructure with Gleeble and measured fracture strain at different locations of the microstructure in HAZ [11]. They divided the HAZ into different regions with fine solid element mesh (~ 0.1 mm), and a calibrated model with tensile specimen and 3-point bending. They could predict failure for element sizes of 1.5 mm and less with 3D solid elements, but did not get satisfying results for larger element sizes.

The current paper will present the experimental procedure for characterization of weld nugget failure and HAZ softening. A homogenous Usibor® 1500 stackup with two thicknesses (1.2 mm and 2.5 mm) has been presented as an example for weld failure prediction and HAZ failure. Weld nugget failure has been simulated by using an eight hexahedral element connected to parent shell elements using a contact card, and two weld failure models were compared - *MAT_100 and *MAT_100_DA. HAZ failure was modeled in 2.5 mm and 1.2 mm Usibor® 1500 stackup for KSII-90, tension-shear and coach-peel loading modes. New stress-strain curves were produced for softened HAZ of Usibor® 1500 using advanced simulation and heat-treatment in Gleeble. Results show the new stress-strain curve from Gleeble can predict yielding of HAZ better, and existing failure criteria in LS-DYNA can predict some loading modes, but not all with bending failure.

2 Experimental Procedure

Materials were welded with Medium Frequency Direct Current (MFDC) to achieve the targeted nugget size as per the FCA standard. Between 100 and 200 welds were performed for each stackup. Nuggets were checked to confirm the minimum diameter threshold was not violated, which in turn was used to ensure weldability robustness and capture the effect of electrode wear. Two weld interfaces were measured for three layer stackups, between middle and upper sheets, and middle and lower sheets.

Mechanical characterization was performed with different loading modes. Cross-tension and tension-shear tests were done as per AWS standard [12]. The coach peel test was used for capturing the effect of bending moment. KSII geometries were tested at three angles - 30, 60 and 90 degrees, called KSII-30, KSII-60 and KSII-90 hereafter, respectively. Figures 1a, b, c and d show the configuration of tests in MTS tensile machine for coach-peel, KSII-30, 60 and 90 degrees respectively. KSII-90 was used to model the axial load in prediction, and as samples are pre-bent, there is no effect of base material bending around the nugget that would otherwise make the prediction model for weld failure complex. While tension-shear and KSII-90 specimens were used to model the almost pure shear and axial loading modes, KSII-30 and KSII-60 were used to model loading modes with a combination of shear and axial forces.

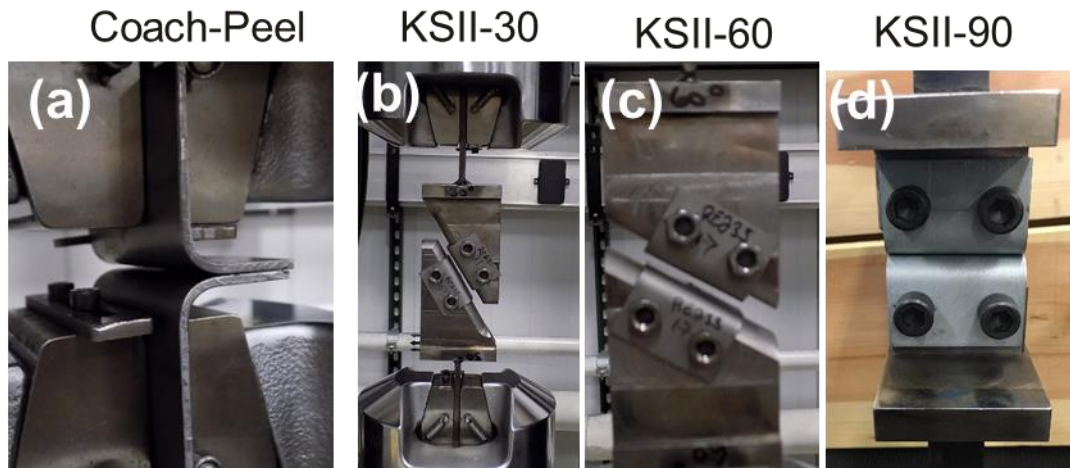


Figure 1 Images of mechanical tests for spot-welded samples at loading modes of (a) coach-peel, (b) KSII-30, (c) KSII-60 and (d) KSII-90.

A unique bending radius of 6.5 mm for pre-bent KSII and coach peel samples was found appropriate to test all AHSS stackups of strengths up to 1500 MPa and thicknesses up to 2.5 mm. For press hardening steels, including Usibor® 1500, the samples were heat-treated first and then bent for different loading modes. The samples were checked for appearance of any crack in the bent areas and no cracks were observed on any sample. Mechanical tests were performed with a displacement rate of 0.4 inch/min. Force-displacement data was acquired from the tensile machine. After mechanical tests were completed, minimum, maximum and average button sizes were measured. Failure modes were recorded, as Interfacial Failure (IF), Partial Interfacial Failure (PIF) or Plug Failure (PF). Interfacial and partial interfacial failures are representative of weld nugget failure in FEA modeling, while plug failure depends on the initiation of failure. Hence, plug failure has been divided into two failure mechanisms - Round Button (RB) where failure starts in front of the notch and propagates through Super Critical HAZ (SCHAZ), and Round Button Heat affected zone (RBH) where the softened HAZ plays the dominant role. Hereafter, RB is associated with spot weld nugget failure modeling, while RBH is associated with HAZ modeling. For spot weld modeling, the minimum weld size targeted for the stackup was obtained in FEA modeling. The weld size would change sample to sample, and it was usually bigger than modeled weld size. Change in weld size resulted in scatter in the failure load. Consequently, the average load-displacement with upper and lower limits of failure load were reported in this paper.

Table 1, shows the example stackups with Usibor® 1500. All of them are three layer heterogeneous stackups, however stackups #1 and #2 are considered to be homogenous as the mild steel strip on the outside does not play a significant role on mechanical properties of the tested specimen. Hereafter, in the paper, stackups #1 and #2 will be referenced as homogenous stackups. Stackups have been called by numbers in first column and referenced hereafter using this number. Table 2, shows the minimum weld size examined in tested specimens and weld strengths for all loading modes - tension shear, coach peel, KSII-30, 60 and 90. Failure mode for all loading modes has been tabulated as well. For example, comparing stackups #2, 3 and 4 with 1.2 mm Usibor® 1500 shows that welding with TRIP690 GI (stackup #4) increases cross-tension strength twice, tension-shear strength is almost similar, but it reduces coach-peel strength by 30% as compared to stackup #2. These results indicate the importance of selection of stackups in the vehicle design depending on the loading mode which the parts undergo during crash test.

Figure 2 shows axial force as a function of shear force for studied stackups. The vertical axis of the graph was plotted from KSII-90 test and the horizontal axis from the tension shear test. The two internal data points were calculated from the decomposition of KSII-30 and 60 test into pure shear and axial forces [11]. As seen, stackup #1 shows a larger failure surface as compared to other stackups. This can be contributed to higher thickness of Usibor® 1500 samples. Figure 2(b) shows all stackups except stackup #1 in a higher resolution. As shown, 2D failure surface configuration is different for each stackup and while a stackup can have higher strength in axial loading mode, it could be less in

shear loading mode, or vice versa. All this information was used for calculating the exponents in *MAT_100 and *MAT_100_DA material card.

Table 1 Three layer heterogeneous stackups with different thickness of Usibor® 1500 examples.

Stackup #	A; Material (Thickness, mm)	B; Material (Thickness, mm)	C; Material (Thickness, mm)
1: A/B/C	Usibor® 1500 (2.5)	Usibor® 1500 (2.5)	CR02 GI (0.7)
2: A/B/C	Usibor® 1500 (1.2)	Usibor® 1500 (1.2)	CR02 GI (0.7)
3: A/B/C	LAH340 GI (1.2)	Usibor® 1500 (1.2)	CR02 GI (0.7)
4: A/B/C	TRIP690 GI (1.2)	Usibor® 1500 (1.2)	CR02 GI (0.7)
5: A/B/C	Usibor® 1500 (1.5)	LAH340 GI (1.2)	TRIP690 GI (1.2)
6: A/B/C	Usibor® 1500 (1.5)	LAH340 GI (1.2)	DP780 GI (1.5)
7: A/B/C	TRIP780 (1.54)	Usibor® 1500 (1.5)	LAH340 GI (1.2)

Table 2 Weld strength and failure modes in different loading modes for example stackups.

Stackup #	MWS (mm)	TS (kN) (FM)	CT (kN) (FM)	CP (kN) (FM)	KSII-30 (kN) (FM)	KSII-60 (kN) (FM)	KSII-90 (kN) (FM)
1	7.5 mm	51 kN (IF)	12 kN (PIF/PF)	2.5 kN (IF/PIF)	27.5 kN (IF)	17.5 kN (PIF/IF)	15 kN (IF)
2	4.5 mm	18 kN (PF)	6 kN (PF)	2 kN (PF)	9.2 kN (PF)	6.3 kN (PF)	6.5 kN (PF)
3	4.5 mm	19 kN (PF)	6.5 kN (PF)	1.6 kN (PF)	8 kN (PF)	6 kN (PF)	6 kN (PF)
4	4.5 mm	19 kN (PF)	11.5 kN (PF)	1.4 kN (PF)	8.9 kN (PF)	9.2 kN (PF)	12 kN (PF)
5	4.5 mm	24.5 kN (IF/PF)	8.3 kN (PF)	2.5 kN (PF)	10.5 kN (IF/PF)	8.6 kN (PF)	8.3 kN (PF)
6	4.5 mm	23 kN (IF)	6.5 kN (PF)	2.3 kN (PF)	NA	NA	NA
7	4.5 mm	13 kN (PF)	6.5 kN (PF)	1.6 kN (PF)	9.0 kN (PF)	8.5 kN (PF)	NA

MWS: Minimum Weld Size in tested specimens, CT: Cross-Tension, TS: Tension-Shear, CP: Coach-Peel, FM: Failure Mode, IF: Interfacial Failure, PIF: Partial Interfacial Failure, PF: Plug failure, NA: Not Available

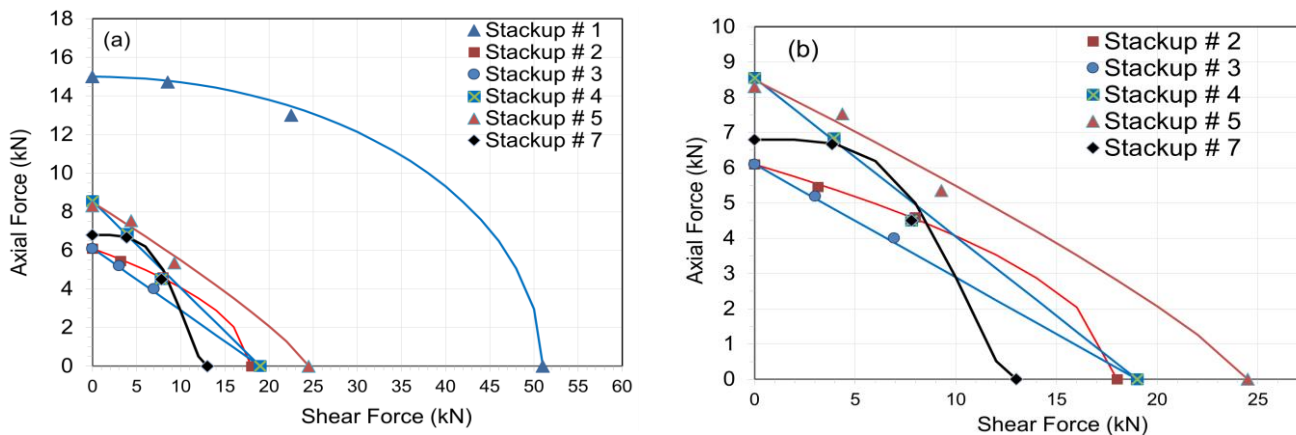


Figure 2 Measured and calculated load bearing capacity split into axial and shear force components for (a) Stackups # 1, 2, 3, 4, 5 and 7 and (b) all except stackups #1 in higher resolution.

A methodology was developed to simulate thermal history and tempering kinetics of martensitic microstructure in subcritical heat affected zone [13]. The sub-critical heat affected zone of spot welds in Usibor® 1500 was simulated, and equivalent heat treatment cycle was designed with similar hardness and microstructure as found in HAZ. This technique produced samples with similar hardness as measured in the actual welds, and the size of the samples was large enough to be tensile tested and consequently produce stress-strain tensile properties for CAE modeling. Figure 3 shows typical Vickers hardness across cross-section metallography of Usibor® 1500. As seen, there is a significant softening in the HAZ which is related to the maximum tempering of martensite microstructure at Ac1 temperature (~720° C). The stress-strain curve was extracted by tensile test on Gleeble specimens simulated from the heat affected zone, which experienced close to maximum softening at Ac1 temperature. Figure 4 shows the stress-strain curve that was used for the HAZ zone shell element in the current study. Also, the base metal uniaxial tensile curve plus base metal tensile curve after scaling with hardness reduction factor of 0.7x have been plotted in Fig. 4. As seen, the yielding point in the HAZ microstructure simulated with Gleeble doesn't decrease as the hardness scale factor curve shows. The strain hardening decreases in HAZ which cannot be otherwise captured with hardness scale factor method.

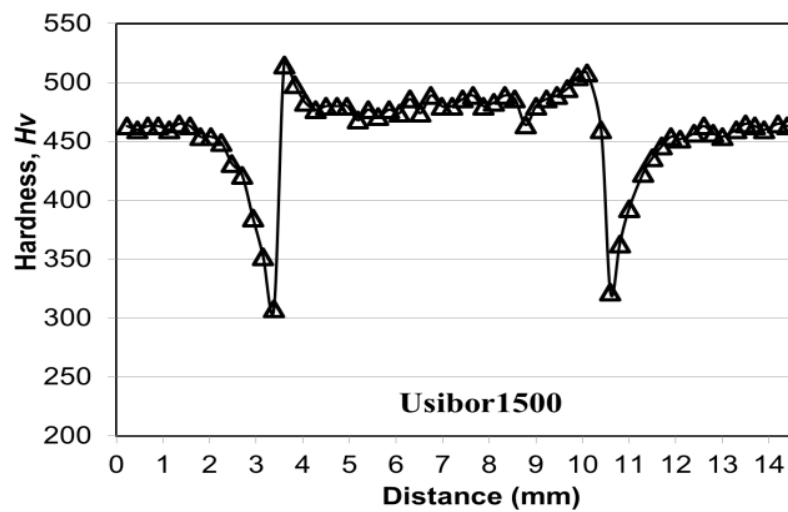


Figure 3 Hardness of Usibor® 1500 from cross-section of spot-welded sample.

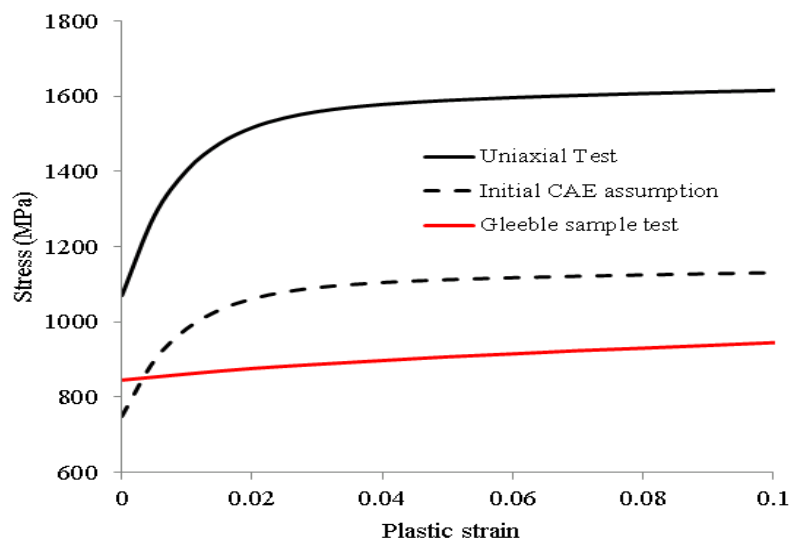


Figure 4 Uniaxial tensile stress-strain curve for Usibor® 1500; Base metal, base metal with scaling factor of 0.7x (initial CAE assumption) and stress-strain curve measured using Gleeble samples simulated from HAZ with minimum hardness

3 Spot-Weld and HAZ Modeling

A paramount goal of the spot weld modeling is to correctly capture the loading environment the spot weld undergoes, so that, in turn it can correctly capture the spot weld failure under combined loading during impact events. An eight, hexahedral element spot weld assembly was used to model the weld nugget as it is a closer representation of the circular physical weld and more suitable to capture local deformation [14]. A contact definition was used to properly capture the load transfer from the sheet metal into the spot weld nugget. Further, the eight, hexahedral spot weld assembly along with the HAZ ring is able to capture the bending due to different loading modes better compared to a one or four, hexahedral representation. Contact between the weld and sheet metal becomes more robust and a minimal pass through from sheet metal into the nugget is observed with an increased number of nodes on the spot weld [15]. An eight, hexahedral spot weld assembly is also preferred in full vehicle simulations for minimum element size and model size. The spot weld and HAZ zone were modeled using the connection manager feature of ANSA pre-processor from BETA CAE. The spot weld was modeled as an assembly of eight, hexahedral elements represented by *DEFINE_HEX_SPOTWELD_ASSEMBLY card in LS-DYNA. The diameter of the weld was used to represent the physical weld area. The HAZ zone diameter was modeled as 0.35 times of the weld diameter.

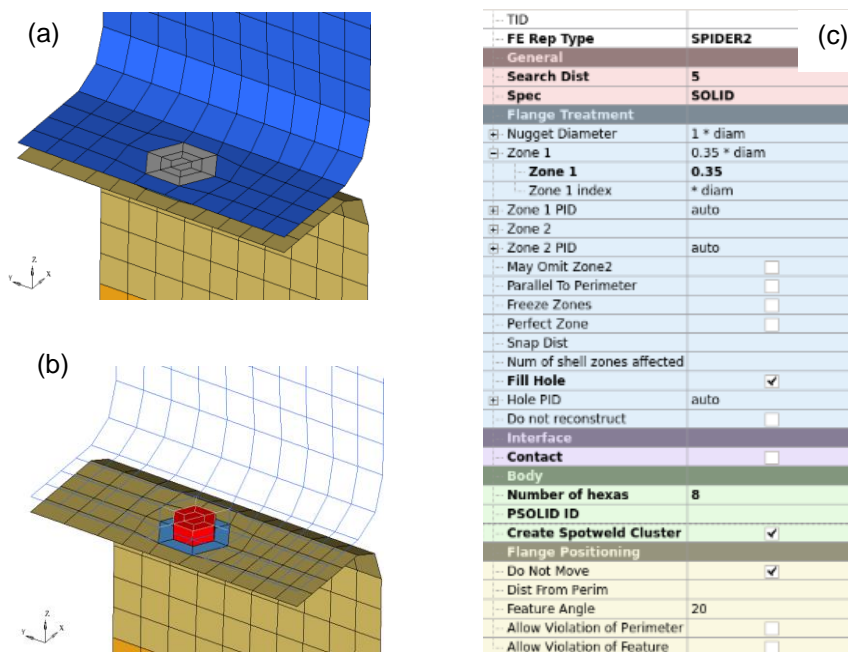


Figure 5 (a) Shell element representation of HAZ, (b) An eight, hexahedral assembly representation of spot weld and (c) Connection manager from BETA-ANSA

A schematic of the HAZ zone, spot weld nugget and the input for the connection manager in BETA ANSA for creating the spot weld assembly and HAZ ring is shown in Fig. 5. A quadrilateral element dominant mesh of 5 mm average size was used for modeling the samples. The element size for the weld and HAZ is guided by the weld diameter input as discussed above.

Figure 6 shows tension shear, KSII-90 and 60 coupons as modeled in CAE. Part 1, 4 were modeled as *MAT_RIGID whereas Part 2, 3 were modeled as deformable components. Further Part 4 was fixed. A 1D spring element attached to part 1 was used to apply the load as shown as in Fig 6. The stiffness of the spring was tuned to account for any compliance in the test fixture.

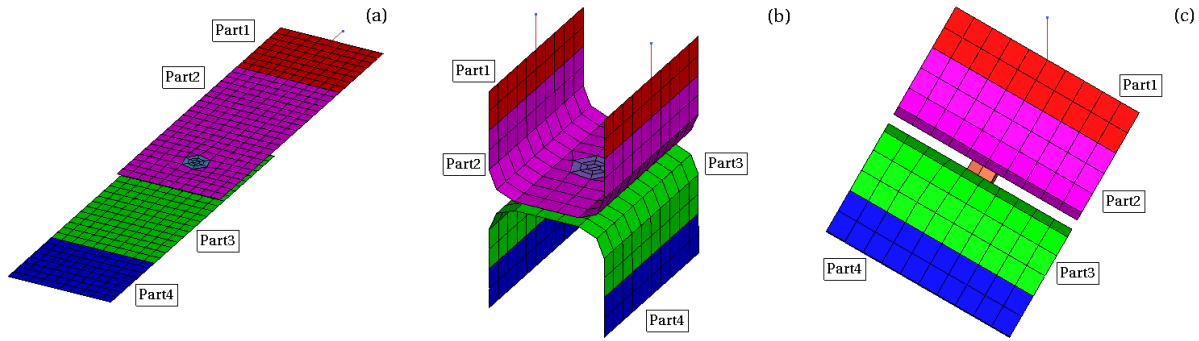


Figure 6 CAE models for (a) tension shear, (b) KSII-90 and (c) KSII-60

In the coupon, for the spot weld, two material models, *MAT_SPOTWELD (*MAT_100) and *MAT_SPOTWELD_DAIMLERCHRYSLER (*MAT_100_DA) with the *DEFINE_CONNECTION_PROPERTIES option were investigated. For parent material & HAZ ring, *MAT_TABULATED_JOHNSON_COOK (*MAT224) was used. The choice of this material model was based on the ability to define a plastic strain vs triaxiality failure curve compared to a single uniaxial tension failure. For HAZ, the stress-strain curve extracted by tensile test on Gleeble specimens simulated from the HAZ as discussed in section 2 (Fig.4) was used. *CONTACT_TIED_SHELL_EDGE_TO_SURFACE card was used to define contact between the weld nugget nodes and the HAZ shell elements. SPOTTHIN = 0.1 and SPOTDEL =1 were used in the *CONTROL_CONTACT card. All other parameters in *CONTROL_CONTACT were left as default from LS-DYNA.

4 Results and Discussion

The preprocessor ANSA has the flexibility to create an eight, hexahedral spot weld assembly using node equivalence, or a tied contact between the hexahedral nugget and shell elements of the joining sheets. Initially, a node equivalence strategy was used between the nugget and shell. It was observed, as the HAZ shell gets deleted, it leaves the nugget without any connection to rest of the model, causing instabilities in full vehicle simulations. This was overcome by using the *CONTACT_TIED_SHELL_EDGE_TO_SURFACE card between the weld nugget and shell elements using SPOTDEL = 1 in *CONTROL_CONTACT card. This ensured that the nugget assembly gets deleted as soon as the HAZ shell connected to it fails, thereby avoiding any instabilities in the model. In the absence of HAZ material data, a 0.7x scale of the parent material stress-strain curve for Usibor® 1500 was used to model HAZ and subsequent Gleeble sample tests revealed a different stress-strain curve for HAZ as shown in Fig.4. It was observed that the stress-strain curve from Gleeble samples was able to predict the yielding in HAZ and result in better correlation to the test, which was not the case otherwise. The maximum effect on the yielding prediction was seen in the tension shear loading mode. A comparison is shown in Fig. 7 for stackup #1, tension shear loading mode using *MAT_100 material card for spot weld.

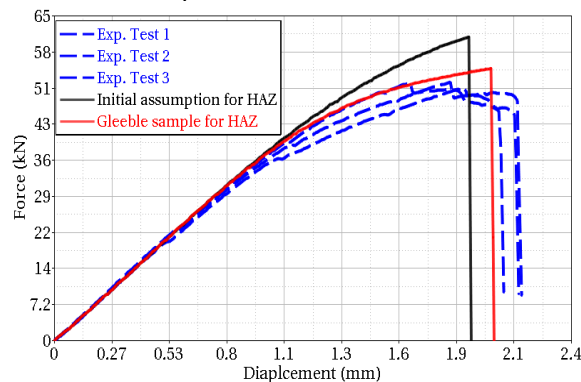


Figure 7 Force-displacement comparison between HAZ stress strain curve from initial CAE assumption and Gleeble samples

Initial CAE simulations with *MAT_100 for spot weld failure provided a reasonable coupon test to CAE correlation for tension shear (shear force), KSII-90 (axial force) and coach peel loading modes. However, KSII-60 and KSII-30 were found to correlate better to test results with *MAT_100_DA as shown in Fig. 8 (stackup #1). It was observed *MAT_100_DA can capture the failure surface defined by these two additional failure points between a pure axial and pure shear force. *MAT_100_DA also has an option to add weld damage, which can capture the additional energy absorbed by the weld in a crash event during damage stage instead of an instant nugget failure and is part of the future study.

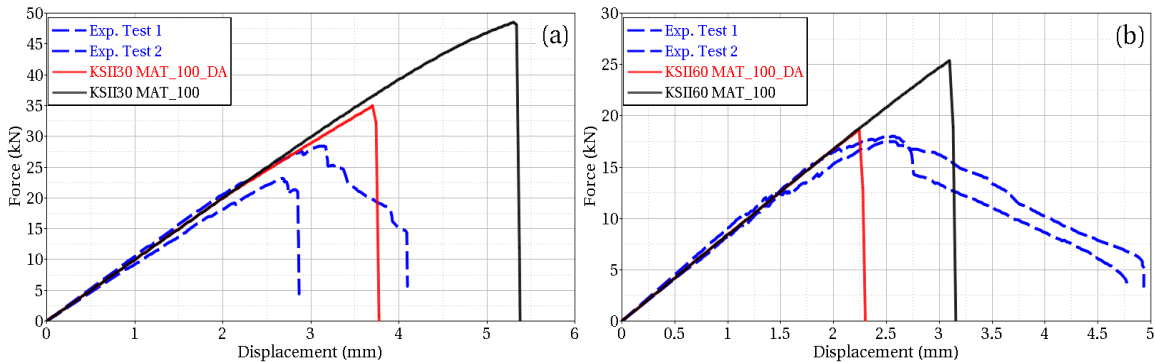


Figure 8 Force-displacement comparison of *MAT_100 and *MAT100_DA in (a) KSII-30, (b) KSII-60

The weld failure in *MAT_100_DA is defined by a stress failure equation as shown in Eq. 4 of section 1. The shear (τ), normal (σ_N) and bending (σ_B) strength components for the failure curve were derived from the test data. The corresponding shear (n_s), normal (n_N) and bending (n_B) exponents were calculated as a best fit solution to the failure equation for correlating all the loading modes as accurately as possible.

DETAN (Tangent modulus for the spot weld) option in the *DEFINE_CONNECTION card was evaluated with two values of 180 GPa, based on the steel properties and 18 GPa, based on the post yielding slope from the mechanical test data of spot-welded samples. There was no difference observed on the coach peel, KSII-90 and KSII-60 loading modes, however, using 18GPa presented a better correlation in the tension shear and KSII-30 loading modes because of higher shear force contribution as shown in Fig. 9 for stackup #1.

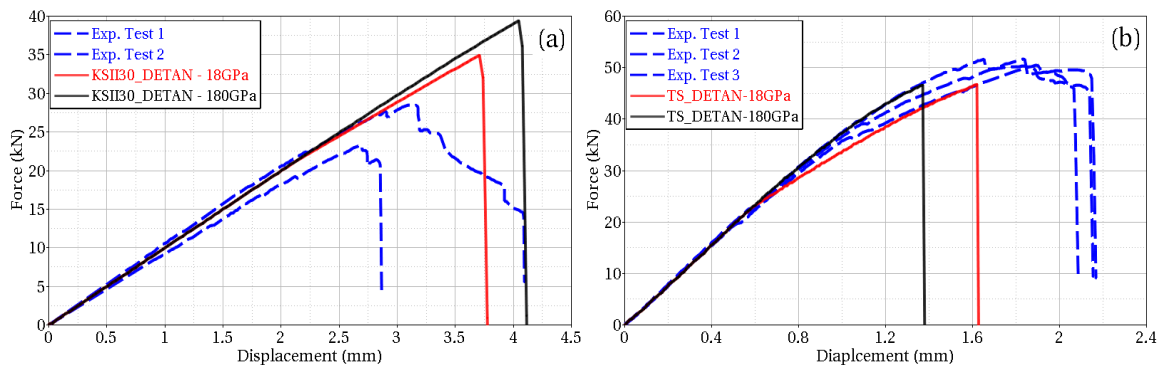


Figure 9 Force-displacement comparison of DETAN effect for (a) KSII-30 and (b) tension-shear.

Figure 10 shows the test to CAE correlation results for all the loading modes in Stackup #1 with only spot weld failure taken into consideration using *MAT_100_DA material card and HAZ stress-strain curves from Gleeble sample testing. A reasonable correlation for maximum failure load was achieved for all loading modes.

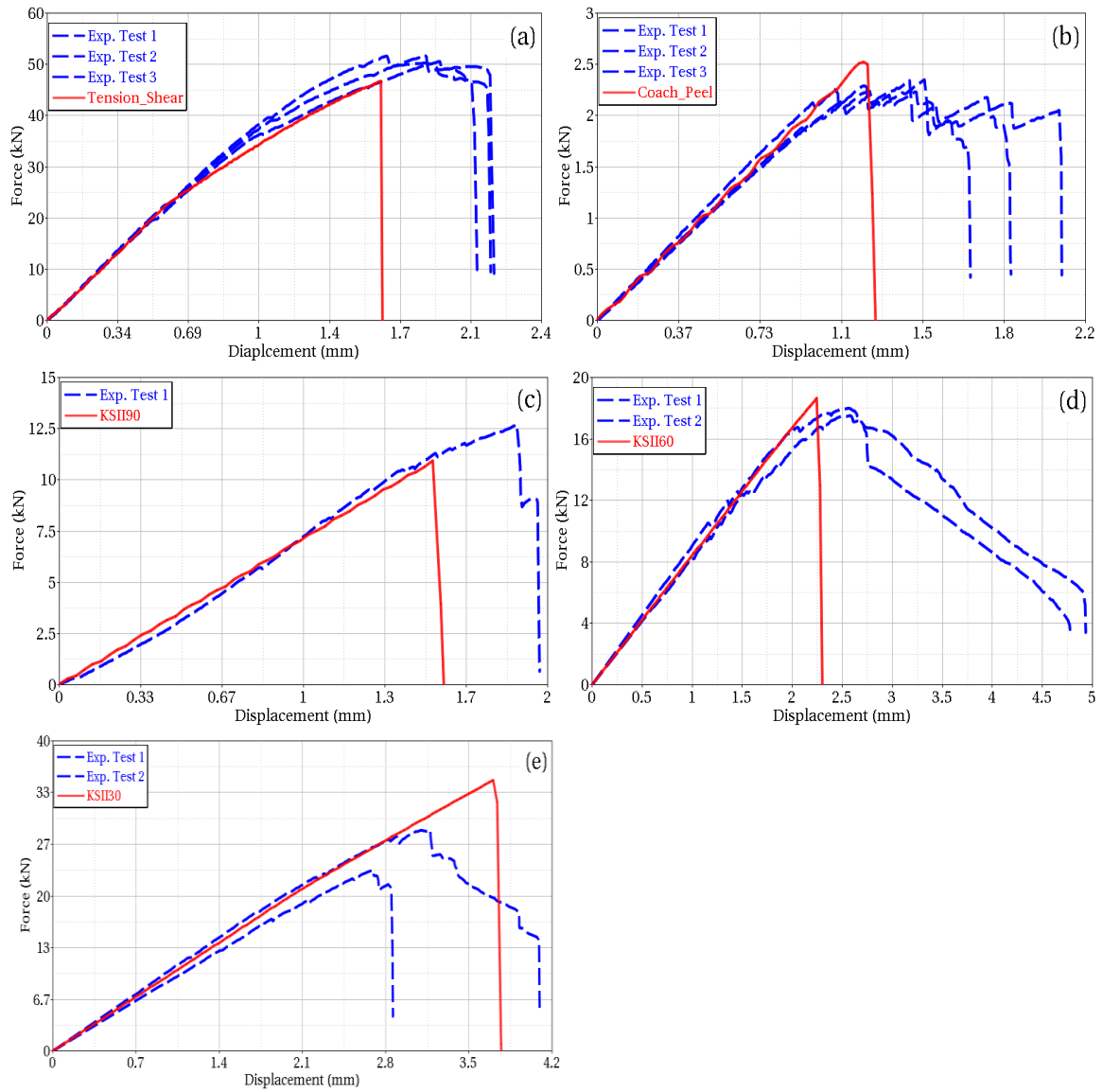


Figure 10 Stackup #1 (2.5 mm Usibor® 1500 homogenous stackup) Force-displacement curve for weld failure in (a) tension shear, (b) coach peel, (c) KSII-90, (d) KSII-60 and (e) KSII-30

A similar test to CAE correlation for weld failure only was observed on Stackup #2 as shown in Fig. 11.

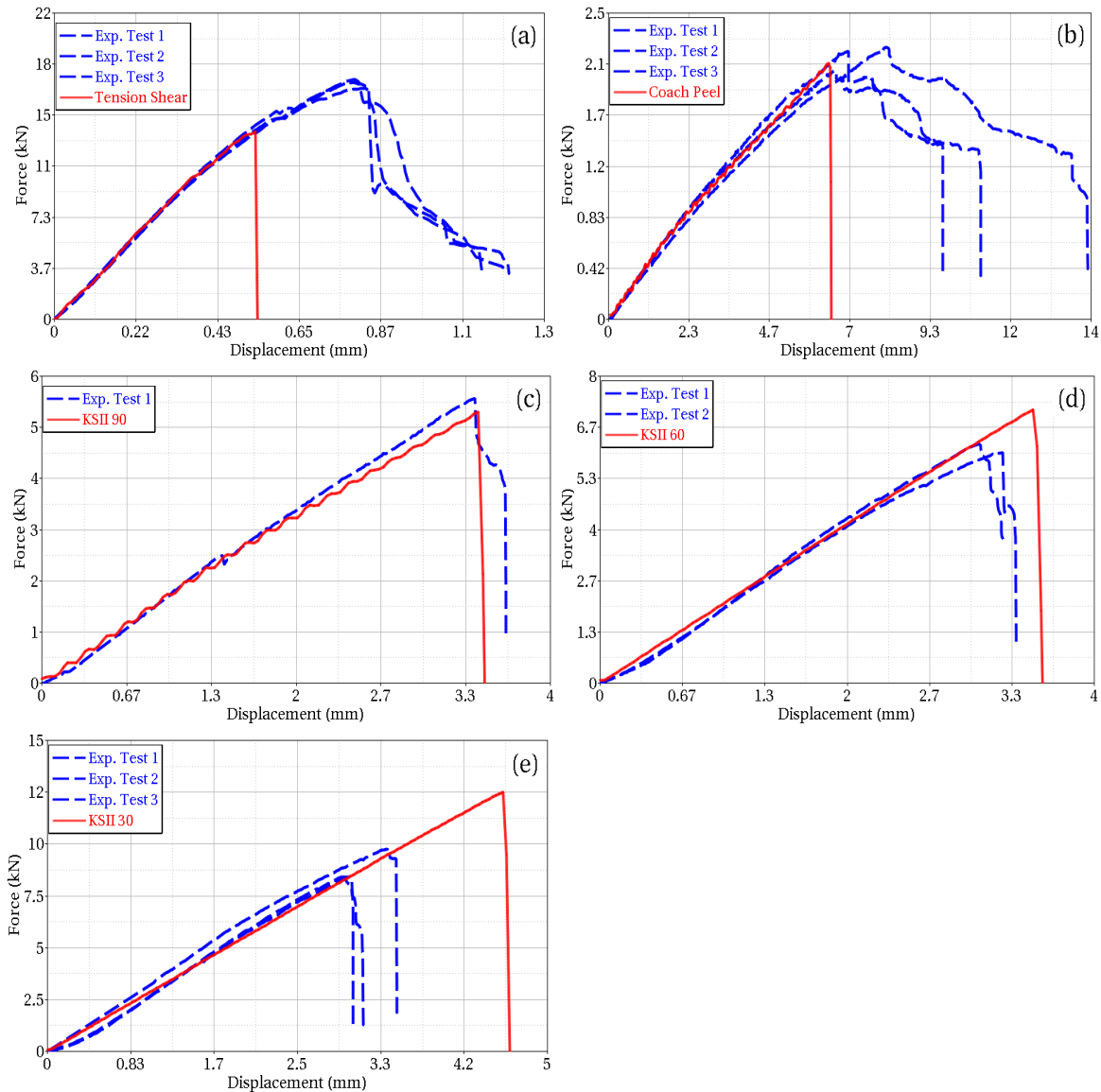


Figure 11 Stackup #2 (1.2 mm Usibor® 1500 homogenous stackup) Force-displacement curve for weld failure in (a) tension shear, (b) coach-peel, (c) KSII-90, (d) KSII-60 and (e) KSII-30

Once a reasonable correlation was achieved for weld failure only, HAZ based failure was evaluated for stackup #2 by reverse engineering the failure from test data. The plastic strain failure and corresponding triaxiality values at the time of failure corresponding to test for each loading mode was extracted from the HAZ elements and HAZ failure curve was modified with extracted data points. A reasonable correlation was observed for tension-shear, coach peel and KSII-90 loading modes as shown in Fig. 12. However, an over prediction in CAE was observed for KSII-30 and 60 loading modes where bending is more dominant. We expect this will be improved with HAZ material modeling in future work.

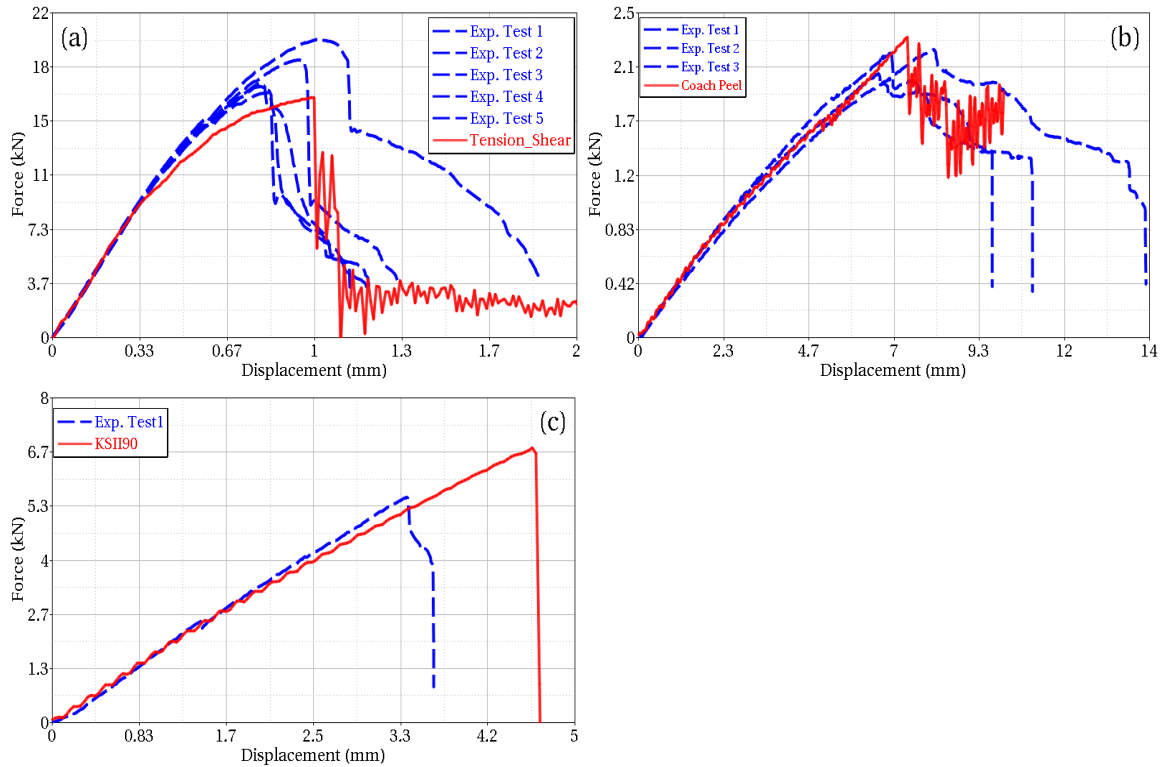


Figure 12 Stackup #2 (1.2 mm Usibor® 1500 homogenous stackup) Force-displacement for HAZ failure in (a) tension-shear, (b) coach-peel and (c) KSII-90

5 Conclusion

To completely understand the physical behavior of spot weld failure, it was necessary to perform the following five unique tests; tension shear, coach peel, KSII-30, 60 and 90. Results from these tests define the spot weld failure surface for various combined spot weld loading conditions in a full vehicle simulation. This paper proposes an eight, hexahedral element spot weld assembly with HAZ, *MAT_100_DA, and contact definition between the joining sheets and spot weld nugget to capture the proper spot weld loading, and in turn, accurate spot weld failure. The Gleeble methodology is recommended for stress strain characterization to capture the yielding of the HAZ of Usibor® 1500, and other high strength steels. This shows a reasonable test to CAE correlation.

The proposed spot weld modeling has been successfully implemented in full vehicle LS DYNA simulations. This allowed for revising and optimizing the vehicle weld layout for various impact load cases. Future work will focus on the implementation of weld damageability available in *MAT_100_DA model and development of triaxiality vs plastic strain failure curves for the HAZ in complex loading modes, e.g. KSII-30 and 60.

Acknowledgment

The authors would like to thank Andrew Morland from FCA for supporting welding of stackups and providing coupons for mechanical tests. We would also like to thank Rob Matakovic from Beta CAE for ANSA support.

6 Literature

1. S. Patil, Modeling and characterization of spot weld material configuration for vehicle crash analysis, Ph. D. Thesis, Wichita State Univ., July 2014.
2. M. Bier, H. Klamser, A. Haufe, 8th European LS-DYNA Conference, 2011.
3. J. H. Lim, J. Ha, and C.Y. Oh, "Practical failure criterion of spot weld for crash simulation", 10th European LS-DYNA Conference 2015, Wurzburg Germany.
4. Y. P. Yang, Sheet Metal Welding Conference XV, 2012.
5. Lee, Y., Wehner, T., Lu, M., Morrisett, T., Pakalnins, E., "Ultimate Strength of Resistance Spot Welds Subjected to Combined Tension and Shear," J. Test. Eval., 26, 1998, pp. 213–219.
6. LS-DYNA. Keyword User's Manual. Version 971, Livermore Software Technology Corporation, Livermore, 2007.
7. T.K. Ellera,b, L. Grevea, M. Andresa, M. Medrickya, H.J.M. Geijselaersb, V.T. Meindersb ,A.H. van den Boogaard: J. of Materials & Processing Technology, 234, 2016, 30.
8. D. P. Norman, Modeling spot-weld fracture using CrashFEM, 9th European LS-DYNA conference, 2013.
9. H. Ghassemi-Armaki, E. Biro, S. Sadagopan: ISIJ (2017), Submitted.
10. T.K. Ellera,b, L. Grevea, M. Andresa, M. Medrickya, H.J.M. Geijselaersb, V.T. Meindersb ,A.H. van den Boogaard: J. of Materials & Processing Technology, 234 (2016), 30.S. Burget, S. Sommer: LS-DYNA Forum, Ulm, 2012.
11. S. Burget, S. Sommer: 13th International Conference on Fracture, Beijing, Chin, 2013,
12. AWS D8.9M; Test methods for evaluating the resistance spot welding behavior of automotive sheet steel materials.
13. E. Biro, H. Ghassemi-Armaki: Sheet Metal Welding Conf. XVII, Michigan, USA, (2016).
14. S. Zilincik, J. DeFrank, E. Monroe, S. Khan, "A New Approach to Evaluating Spot Welds for Automotive Durability", SAE International, 1998.
15. S. Malcolm, E. Nutwell: 6th European LS-DYNA User Conference, 2015.